Faraday Discussions

Cite this: *Faraday Discuss.*, 2017, **200**, 121

PAPER

Aerosol climate change effects on land ecosystem services

N. Unger, *[a] X. Yue[b] and K. L. Harper[c]

Received 23rd January 2017, Accepted 24th February 2017
DOI: 10.1039/c7fd00033b

A coupled global aerosol–carbon–climate model is applied to assess the impacts of aerosol physical climate change on the land ecosystem services gross primary productivity (GPP) and net primary productivity (NPP) in the 1996–2005 period. Aerosol impacts are quantified on an annual mean basis relative to the hypothetical aerosol-free world in 1996–2005, the global climate state in the absence of the historical rise in aerosol pollution. We examine the separate and combined roles of fast feedbacks associated with the land and slow feedbacks associated with the ocean. We consider all fossil fuel, biofuel and biomass burning aerosol emission sources as anthropogenic. The effective radiative forcing for aerosol–radiation interactions is −0.44 W m^{-2} and aerosol–cloud interactions is −1.64 W m^{-2}. Aerosols cool and dry the global climate system by −0.8 °C and −0.08 mm per day relative to the aerosol-free world. Without aerosol pollution, human-induced global warming since the preindustrial would have already exceeded the 1.5 °C aspirational limit set in the Paris Agreement by the 1996–2005 decade. Aerosol climate impacts on the global average land ecosystem services are small due to large opposite sign effects in the tropical and boreal biomes. Aerosol slow feedbacks associated with the ocean strongly dominate impacts in the Amazon and North American Boreal. Aerosol cooling of the Amazon by −1.2 °C drives NPP increases of 8% or +0.76 ± 0.61 PgC per year, a 5–10 times larger impact than estimates of diffuse radiation fertilization by biomass burning aerosol in this region. The North American Boreal suffers GPP and NPP decreases of 35% due to aerosol-induced cooling and drying (−1.6 °C, −0.14 mm per day). Aerosol–land feedbacks play a larger role in the eastern US and Central Africa. Our study identifies an eco-climate teleconnection in the polluted earth system: the rise of the northern hemisphere mid-latitude reflective aerosol pollution layer causes long range cooling that protects Amazon NPP by 8% and suppresses boreal NPP by 35%.

[a]*College of Engineering, Mathematics and Physical Sciences, University of Exeter, Exeter, EX4 4QE, UK. E-mail: N.Unger@exeter.ac.uk*

[b]*Climate Change Research Centre, Institute of Atmospheric Physics, Chinese Academy of Sciences, Beijing 100029, China*

[c]*School of Forestry and Environmental Studies, Yale University, New Haven, CT 06511, USA*

1. Introduction

Gross primary productivity (GPP) is the amount of carbon dioxide (CO_2) removed from the atmosphere by photosynthesis every year. GPP drives the global carbon cycle and is the basis of all food production on planet Earth. Net primary productivity (NPP), the difference between GPP and plant autotrophic respiration (R_a), provides a useful indicator of land carbon uptake and ecosystem health. GPP and NPP are estimated to be about 120 PgC per year[1] and 63 PgC per year,[2] respectively. Understanding human impacts on the land ecosystem services GPP and NPP is critical for sustainable use of the land biosphere and future climate safety. Plant isoprene emission is an abiotic stress function related to the protection of photosynthetic capacity during high temperatures.[3–5] Isoprene is produced in the chloroplast from precursors formed during photosynthesis. The estimated global source of isoprene from plants to the atmosphere is about 0.5 PgC per year.[6]

GPP, NPP and isoprene emission have differing and complex sensitivities to physical climate change.[7] Land carbon–climate feedbacks are the subject of intensive research[8–11] because future global and regional climate change over the 21st century depends on the rate at which anthropogenic CO_2 emissions are removed from the atmosphere by the land carbon sink.[10] At the global-scale, GPP decreases with rising temperature, which contributes to the negative land carbon–climate feedback sensitivity estimated to be -58.4 ± 28.5 PgC per °C.[12] In tropical and temperate ecosystems, the land carbon storage has a negative relationship with increasing temperature, in contrast to boreal ecosystems that have a strong positive relationship.[7] Precipitation controls GPP in more than 40% of vegetated land, and radiation control plays an important role in boreal ecosystems.[1,13] The isoprene response to physical climate change must reflect a signature of the GPP response.[14,15] However, isoprene emission has higher temperature and light optimums than photosynthesis, such that at high leaf temperature and light exposures, the rate of isoprene production and photosynthesis are inversely correlated.[16,17] This behavior of isoprene emission suggests an increase in a warmer physical climate state.[18]

Human activities since the industrial and agricultural revolutions have led to an increase in aerosol loading concentrated in the NH mid-latitudes and over tropical biomass burning regions. Globally, this aerosol pollution is estimated to cause about 3.3 million premature deaths per year worldwide.[19] The rise of atmospheric aerosols through the industrial era has altered the global physical climate state in distinctly different ways from CO_2 and the other well-mixed greenhouse gases (WMGHGs).[20] In the initial step, anthropogenic aerosols interact with the atmospheric radiation budget; most anthropogenic aerosol particles (sulfate, nitrate, organic carbon) scatter solar radiation back to space and lead to net global cooling, while black carbon absorbs solar radiation and warms the planet.[21] Aerosols modify cloud properties by affecting cloud microphysical processes.[20] Then, as the earth system responds to the radiative energy imbalance imposed by the atmospheric aerosol loading, physical climate change occurs on a range of spatiotemporal scales. Aerosol-induced physical climate change can broadly be separated into: (i) fast feedbacks associated with the land–atmosphere system adjusting to the aerosol radiative perturbation (days to years)

and (ii) slow feedbacks associated with the ocean–atmosphere system adjusting to the aerosol radiative perturbation (decades to centuries). The combined response is not expected to be the exact linear sum of (i) and (ii) due to dynamical coupling mechanisms between land, atmosphere and ocean. The land–atmosphere fast feedbacks are equivalent to the effective radiative forcing (ERF) defined in the IPCC AR5.[21] ERF is the change in net top of the atmosphere (TOA) downward radiative flux after allowing for atmospheric and land temperatures, water vapor and clouds to adjust. ERF is calculated by fixing sea surface temperatures (SSTs) and sea ice cover at climatological values while allowing all other parts of the system (land–atmosphere) to respond until reaching steady state.

Incorporating both land and ocean feedbacks, global climate models suggest that anthropogenic aerosols have cooled the global temperature by about 1 °C relative to the preindustrial,[22,23] masking approximately 50% of the global warming caused by carbon dioxide (CO_2) and other WMGHGs.[24,25] Aerosols have larger impacts on regional precipitation changes than WMGHGs, but the effects tend to be model dependent.[26,27] A robust impact of the interhemispheric asymmetry in net reflective aerosol radiative forcing, which is concentrated in the northern hemisphere (NH), is the shift in tropical precipitation toward the relatively warming southern hemisphere (SH).[28]

Even though aerosols impose a large cooling effect on the global climate state today, effectively restraining CO_2-induced global warming, the impacts and relevance for land ecosystem services are not well understood. A few global coupled climate–carbon cycle modeling studies begin to isolate aerosol physical climate change effects on the global carbon cycle.[29–32] Simulations with the HadCM3 Earth System Model suggested vegetation carbon increases of 0.5 to 6 kgC m^{-2} in the Amazon, and decreases of -0.5 to -3 kgC m^{-2} in the boreal zone, for the 1970–2000 average period, due to sulfate aerosol cooling.[29] Applying the same model framework, Cox *et al.* found that future reductions over the coming century in reflective aerosol pollution in the NH mid-latitudes increase the risk of severe drought conditions in the Amazon, similar to those experienced in 2005.[30] The dominant impact of aerosols on the carbon cycle likely occurs through cooling the climate, which acts to increase the land and ocean carbon sinks, and represents an indirect CO_2 radiative forcing of -0.02 to -0.24 W m^{-2}.[32]

Most research to date on aerosol–carbon cycle interactions focuses on aerosol diffuse radiation fertilization rather than global cooling.[33–41] For example, a recent study suggested that biomass burning aerosols in the Amazon increase the annual mean diffuse light and NPP by 3.4–6.8% and 1.4–2.8%, respectively.[39] Similarly, Strada and Unger (2016) found that biomass burning aerosols increase annual GPP by 2–5% in the Amazon and that anthropogenic aerosols enhance annual GPP by 5–8% in the eastern United States (US).[40] The model framework included bio-meteorological feedbacks from the aerosol-influenced vegetation physiology, but used fixed canopy structures and phenology. It is not possible to change the light environment without altering the climatic conditions.

The Coupled Model Intercomparison Project (CMIP) land carbon–climate experimental design is based on 1% per year increases in CO_2 and does not consider anthropogenic aerosols. Trends and attribution studies apply meteorological reanalysis data that embeds both WMGHG and aerosol influences.[2] Since aerosols have fundamentally different impacts on surface radiation, temperature and precipitation than CO_2 and WMGHGs, and given the probable future aerosol

removal due to public health concerns, there is a need to improve understanding of aerosol climate change impacts on land ecosystem services. This study employs the NASA ModelE2-YIBs global aerosol–carbon–climate model[42] to quantify the impacts of persistent anthropogenic aerosol forcing on the land ecosystem services: GPP, R_a, NPP, and isoprene emission. The study period is the 1996–2005 decadal average. We define the "aerosol-free" world as the hypothetical 1996–2005 global climate state in the absence of the historical rise in anthropogenic aerosol loading. Aerosol impacts are analyzed relative to this aerosol-free world, not the preindustrial. The goals are to assess the separate roles of the fast feedbacks associated with the aerosol-induced land energy changes, the slow feedbacks associated with the aerosol-induced ocean energy changes, and the combined influences of the land and ocean feedbacks. The model incorporates interactive oxidants and aerosols, physical climate, and dynamic land carbon allocation and phenology, such that land ecosystem structure and the atmospheric aerosol composition coevolve. This study does not address anthropogenic changes in dust aerosol or the biogeochemical impacts of aerosol deposition on the land biosphere.[31] The model does not include permafrost carbon.

2. Methods

2.1 NASA ModelE2-YIBs aerosol–carbon–climate model

The Yale Interactive Terrestrial Biosphere Model (YIBs) has been embedded inside the NASA ModelE2 global aerosol–climate model[43] in a framework known as NASA ModelE2-YIBs.[42] The framework fully integrates the land carbon–oxidant–aerosol system such that these components interact with each other and with the physics of the climate model. Simulated meteorological and hydrological variables have been validated against observations and reanalysis products.[43] Simulated surface solar radiation demonstrates the lowest model-to-observation biases compared with 20 other IPCC-class global climate models.[44] The global climate model provides the meteorological drivers to YIBs, and the land-surface hydrology submodel provides the grid cell level soil characteristics. This study applies $2^\circ \times 2.5^\circ$ latitude by longitude horizontal resolution with 40-vertical layers extending to 0.1 hPa. The vegetation is described using 8 ecosystem types: tundra, C3 grassland, C4 grassland, shrubland, deciduous broadleaf forest, evergreen needleleaf forest, tropical rainforest, and C3 cropland. We use the satellite-derived global vegetation cover dataset for the present day from the Community Land Model (CLM) that is based on retrievals from both the Moderate Resolution Imaging Spectroradiometer (MODIS) and the Advanced Very High Resolution Radiometer (AVHRR).[45]

2.1.1 The Yale Interactive Terrestrial Biosphere Model (YIBs). YIBs simulates dynamic land carbon assimilation, allocation, and autotrophic and heterotrophic respiration. YIBs biophysics applies the Farquhar, Ball, and Berry coupled photosynthesis and stomatal conductance leaf models for C3 and C4 plants.[46–48] The model vertically stratifies each canopy into diffuse and direct light levels using an adaptive number of layers (typically 2–16).[49] The assimilated carbon is dynamically allocated and stored to support leaf development (changes in leaf area index, LAI) and tree growth. Dynamic daily LAI is simulated based on carbon allocation and temperature- and drought-dependent prognostic phenology.[42] YIBs incorporates 2 isoprene emission algorithms: (1) ISO-P: isoprene emission is

calculated as a function of electron transport-limited photosynthesis, intercellular and atmospheric CO_2 and canopy temperature;[50] and (2) ISO-M: isoprene emission is calculated using empirical functions of canopy temperature and light commonly applied in The Model of Emissions of Gases and Aerosols from Nature (MEGAN).[6] MEGAN is the most widely used system for estimating isoprene emissions from terrestrial ecosystems. The YIBs model has been benchmarked and evaluated using land carbon flux measurements from 145 flux tower sites and multiple satellite products.[42,51,52] At the site level, YIBs simulates reasonable seasonality (correlation coefficient $R > 0.8$) of gross primary productivity (GPP) at 121 out of 145 sites with biases in magnitude ranging from −19% to 7% depending on ecosystem type.[52]

2.1.2 NASA ModelE2 aerosol–climate model. The mass-based aerosol module includes simulation of sulfate, black carbon, primary organic matter, nitrate, biogenic secondary organic aerosol (BSOA), sea-salt, and mineral dust.[43] NO_x-dependent BSOA production from the oxidation of biogenic volatile organic compound (BVOC) emissions (isoprene, monoterpene and other VOCs) is calculated using a 2-product scheme that describes partitioning of semi-volatile compounds between the gas and aerosol phases depending on their volatility and pre-existing carbonaceous aerosol availability.[53,54] Aerosols are treated as externally mixed and have prescribed size and optical properties. The aerosol optical thickness and radiative forcing calculations are based on Mie code embedded in the GCM. Sulfate, nitrate and BSOA radiative parameters (including particle size, density and refractive index) depend on relative humidity, and include formulation for deliquescence.[55] Effective radii (dry) are assumed to be 0.15 μm for sulfate and nitrate, and 0.2 μm for BSOA. The impact of the first aerosol indirect effect on clouds is parameterized according to a simple budget of unactivated cloud condensation nuclei.[56] On-line aerosols provide surfaces for chemical reactions and influence photolysis rates, and on-line oxidants affect photochemical formation of secondary aerosols. Tropospheric oxidation chemistry includes NO_x–HO_x–O_x–CO–CH_4 chemistry as well as peroxyacyl nitrates and the hydrocarbons: isoprene, terpenes, alkyl nitrates, aldehydes, alkenes, and paraffins. The gas-phase chemical oxidation scheme includes 156 chemical reactions among 51 species. Photolysis rates are calculated using the Fast-J2 scheme,[57] which takes into account the model distribution of clouds, aerosols and ozone.[58] The present-day atmospheric composition model has been well tested against observations and compared with other models.[59–62] NASA ModelE2-YIBs simulated aerosol optical depth (AOD) demonstrates skill in comparison against MODIS AOD ($R = 0.7$ and RMSE $= 0.05$); global boreal summer average agreement is as high as $R = 0.8$ and RMSE $= 0.06$.[40]

2.2 Simulations

A total of 4 fully coupled land–atmosphere time-slice simulations are performed in which the land ecosystem structure and atmospheric composition coevolve (Table 1). All simulations allow the online interactive aerosols to impact atmospheric radiation and influence dynamics and meteorology. A present day control simulation (CTRL) applies observed decadal average (1996–2005) monthly varying sea surface temperatures (SSTs) and sea ice fields from the Hadley Centre Sea Ice and Sea Surface Temperature data set (HadISST).[63] Anthropogenic and biomass

Table 1 Summary of simulation experiments

Name	SSTs and sea ice 1996–2005 monthly varying decadal average	Anthropogenic and biomass burning precursor emissions year 2000	Purpose of [CTRL − Sim0X]
CTRL	HadISST obs	Yes	N/A
Sim01	HadISST obs	No	Isolate impacts of aerosol fast feedbacks "AEROSOL–LAND"
Sim02	HadISST obs + CMIP5 [histGHG − histALL] anomalies	Yes	Isolate impacts of aerosol slow feedbacks "AEROSOL–OCEAN"
Sim03	HadISST obs + CMIP5 [histGHG − histALL] anomalies	No	Isolate impacts of aerosol fast + slow feedbacks "AEROSOL–ALL"

burning emissions of reactive gases and aerosols are from the IPCC AR5 global gridded inventory for the year 2000.[64] WMGHG concentrations are prescribed to year 2000 values in the radiation submodel (CO_2 = 369 ppmv; N_2O = 316 ppbv; CH_4 = 1774 ppbv). Atmospheric CO_2 is held constant at 369 ppmv in YIBs. In the atmospheric composition submodel, CH_4 is prescribed to 1814 ppbv in the NH and 1733 ppbv in the SH. A sensitivity simulation (Sim01) is performed that is identical to CTRL but removes all anthropogenic and biomass burning emissions of short-lived gases and aerosols.

Next, SST and sea ice fields are constructed that represent today's global climate state in the absence of the historical rise in anthropogenic aerosols. The CMIP5 provided a set of past transient simulations integrated from 1850 to 2005: (i) "histALL" includes all transient anthropogenic and natural forcings; (ii) "histGHG" includes transient forcings of WMGHGs. We extract decadal average (1996–2005) monthly varying SSTs and sea ice residual anomalies [histGHG minus histALL] from 10 CMIP5 models that incorporated prognostic cloud microphysics and aerosol–cloud microphysics interactions.[28] This method has been used in previous CMIP5-based analyses because the aerosol radiative forcing is 3–4 times larger than other non-WMGHGs, and the climate responses to forcings are approximately linearly additive.[28,65,66] The residual anomalies are added to the 1996–2005 observed HadISST SST and sea ice fields. A second sensitivity simulation (Sim02) is performed that is identical to CTRL except forced with the modified SST and sea ice fields. A final sensitivity simulation (Sim03) is performed that is identical to Sim02 except removes all anthropogenic and biomass burning emissions of short-lived gases and aerosols.

All simulations are run for 40 years to allow the land–atmosphere climate state and aboveground carbon to reach steady state. The last 20 years are averaged for analyses. The difference [CTRL minus Sim01] isolates the fast feedback aerosol climate change effects associated with the land–atmosphere system, referred to as "AEROSOL–LAND"; the difference [CTRL minus Sim02] isolates the slow feedback aerosol climate change effects associated with the ocean–atmosphere system, referred to as "AEROSOL–OCEAN"; the difference [CTRL minus Sim03] isolates the aerosol climate change effects associated with both the land–atmosphere and

ocean–atmosphere systems combined referred to as "AEROSOL–ALL". For all cases, vegetation physiology, leaf phenology and land carbon allocation respond to the aerosol-induced climate change. The standard deviations of the aerosol impacts are calculated based on interannual climate variability for $n = 20$ model years. We present results that are statistically significant at 95% confidence level.

3. Results

3.1 Aerosol radiative effects at TOA

The total ERF for aerosol–radiation interactions is -0.44 ± 0.03 W m^{-2}, close to the IPCC AR5 estimate of -0.45 ± 0.5 W m^{-2} for preindustrial to present day changes.[21] Individual ERFs for aerosol–radiation interactions are: sulfate = -0.32 W m^{-2}; nitrate = -0.17 W m^{-2}; fossil and biofuel black carbon = 0.20 W m^{-2}; fossil and biofuel organic carbon = -0.06 W m^{-2}; biomass burning black carbon = 0.13 W m^{-2}; biomass burning organic carbon = -0.11 W m^{-2}. Anthropogenic short-lived pollution emissions drive a BSOA ERF of -0.10 W m^{-2}. Thus, the presence of anthropogenic aerosol pollution in the climate system causes an increased loading of BSOA, discussed further in Section 3.5.[54,67] The standard deviation of ERFs based on interannual variability is less than 5% for all aerosols, except for BSOA (~30%). Using the calculated changes in the net solar and thermal radiation at TOA, we estimate the total ERF for aerosol–cloud interactions to be -1.64 ± 0.25 W m^{-2}, slightly larger than a median estimate of -1.4 W m^{-2} provided by the IPCC AR5 based on 14 published studies since AR4.[20] This discrepancy occurs because the present model includes aerosol interactions with liquid-phase clouds only, and neglects possible interactions with mixed-phase and ice clouds. In summary, the model provides a realistic interactive global distribution and forcing of scattering and absorbing aerosols from human activities.

3.2 Aerosol impacts on surface visible radiation

Annual average impacts of anthropogenic aerosols on the direct, diffuse and total surface visible radiation are shown for the 3 feedback cases in Fig. 1. AEROSOL–LAND feedbacks govern the changes to surface radiation. The aerosol-induced changes in the quantity and quality of surface radiation are concentrated around the industrial pollution and biomass burning land regions. At the global-scale, aerosols decrease annual average direct surface visible radiation by 8.73 ± 0.40 W m^{-2} (-11%) and increase diffuse surface visible radiation by 2.32 ± 0.52 W m^{-2} (1–2%), resulting in a change to total surface visible radiation of -6.42 ± 0.33 W m^{-2} (-3%) in good agreement with other estimates.[68]

We define 4 key land regions for further analyses shown in Fig. 1: Amazon (53W–75W; 10S–5N), Central West Africa, CW-Africa (10–25E; 10S–10N), Eastern US, E-US (70–95W; 30–50 N) and North American Boreal, NA-Boreal (60W–165W; 56N–73N). Fig. 2 presents a summary of the annual average regional changes to surface visible radiation. In the Amazon, aerosols decrease annual average direct surface visible radiation by 11.04 ± 0.97 W m^{-2} (-11%), increase diffuse surface visible radiation by 2.11 ± 1.42 W m^{-2} (2%), and decrease total surface visible radiation by 8.93 ± 1.04 W m^{-2} (-4%). Larger reductions in annual average direct surface visible radiation occur in CW-Africa of -23.49 ± 1.06 W m^{-2} (-36%)

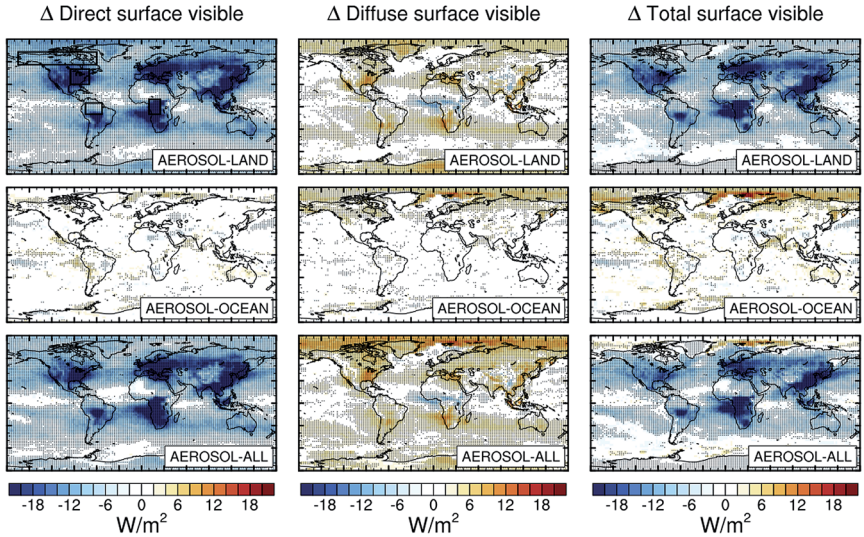

Fig. 1 Spatial distribution of annual average aerosol impacts on direct, diffuse and total visible radiation at the surface for the 3 feedback cases relative to aerosol-free world in 1996–2005 (W m^{-2}). Dots indicate areas where aerosol impacts are statistically significant at the 95% confidence level. The 4 key regions are defined in the top left panel: Amazon, Central West Africa (CW-Africa), Eastern US (E-US), and North American Boreal (NA-Boreal).

accompanied by a decrease in diffuse surface visible radiation by 1.50 ± 1.47 W m^{-2} (−1%) resulting in a change to total surface visible radiation of −24.99 ± 1.01 W m^{-2} (−13%). These reductions are predominantly due to the large loading of absorbing biomass burning aerosol in this region. The E-US experiences stronger conversion of direct to diffuse light than tropical regions. Aerosols decrease annual average direct surface visible radiation by 22.33 ± 2.16 W m^{-2} (−28%) and increase diffuse surface visible radiation by 7.70 ± 3.53 W m^{-2} (5%) resulting in a change to total surface visible radiation of −14.63 ± 2.80 W m^{-2} (−7%). In NA-Boreal, aerosols decrease annual average direct surface visible radiation by 9.29 ± 1.40 W m^{-2} (−19%) and increase diffuse surface visible radiation by 4.91 ± 2.66 W m^{-2} (3%) resulting in a change to total surface visible radiation of −4.39 ± 2.26 W m^{-2} (−2%). The largest absolute and fractional increases in diffuse radiation due to aerosols occur in E-US and NA-Boreal.

3.3 Aerosol impacts on surface climate

Fig. 3 shows the annual average aerosol impacts on surface air temperature (SAT), canopy temperature (CanT) and precipitation for the 3 feedback cases relative to the aerosol-free world in 1996–2005. Aerosols are cooling and drying the global climate state. Global annual average SAT is decreased by 0.78 ± 0.04 °C, CanT by 1.26 ± 0.11 °C, and precipitation by 0.08 ± 0.01 mm per day. At the global-scale, AEROSOL–OCEAN feedbacks dominate the aerosol effects on surface climate. NASA GISTEMP indicates that global warming in 1996–2005 relative to 1880–1889 was already 0.75 °C.[69] Therefore, we estimate that without the simultaneous rise

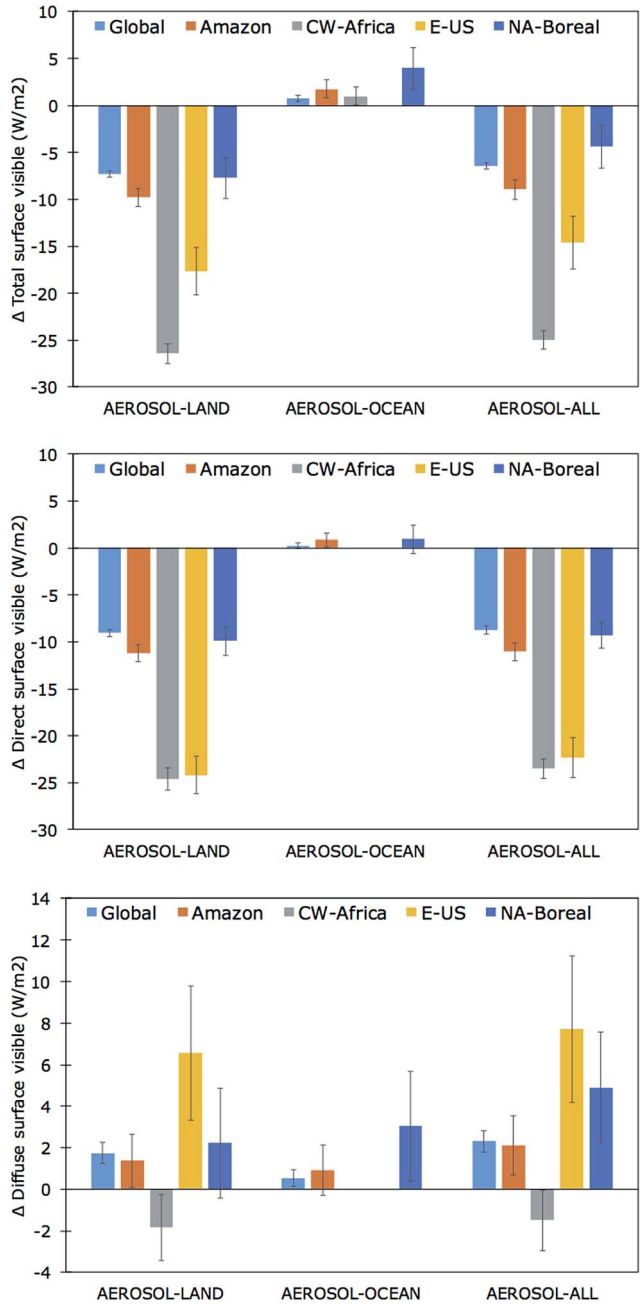

Fig. 2 Summary of annual average aerosol impacts on direct, diffuse and total visible radiation in 4 key regions and globally for the 3 feedback cases relative to aerosol free world in 1996–2005 (W m^{-2}). Vertical axes have different scales. Error bars represent ±1 standard deviation due to interannual variability in the climate model calculated as standard error of the mean based on 20 model years.

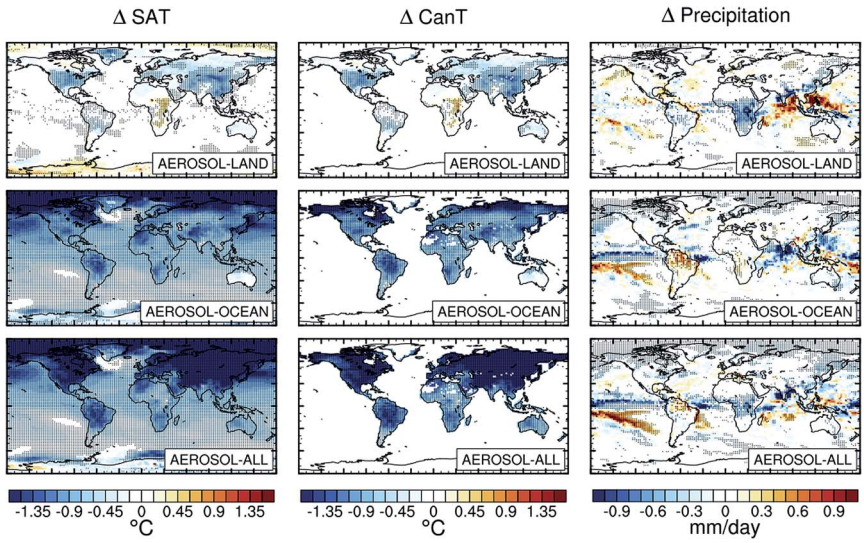

Fig. 3 Spatial distribution of annual average aerosol impacts on surface air temperature (SAT, °C), canopy temperature (CanT, °C), and precipitation (mm per day) for the 3 feedback cases relative to aerosol-free world in 1996–2005. Dots indicate areas where aerosol impacts are statistically significant at the 95% confidence level.

of anthropogenic aerosols, human-induced global warming would have exceeded 1.5 °C, the aspirational limit set in the Paris Agreement, more than a decade ago.

Aerosol feedbacks from energy exchange with the ocean drive strong cooling in the NH high-latitudes and over land masses, essentially the reverse of regional patterns in CO_2-induced warming. AEROSOL–LAND feedbacks drive weaker cooling that is widespread over the NH mid-latitude continents. Aerosols cause cooler canopies across global ecosystems that mirror changes in SAT. The aerosol-driven shift in large-scale tropical precipitation from the NH into the SH agrees quantitatively with a previously published estimate.[28] This meridional shift in the intertropical convergence zone (ITCZ) occurs in order to restore the vertically integrated atmospheric energy budget in response to an anomalous energy imbalance imposed in one hemisphere. The Hadley circulation anomaly manifests as a shift in the ITCZ tropical rain belt toward the warmer hemisphere.[70–72]

Regionally, annual average aerosol-induced changes in surface climate are much larger than the global impacts (Fig. 4). For SAT, CanT and precipitation, the linear sum of AEROSOL–LAND and AEROSOL–OCEAN is within 10% of AEROSOL–ALL for all regions except CW-Africa and E-US. Aerosols decrease annual average SAT in the Amazon, CW-Africa, E-US and NA-Boreal by 1.17 ± 0.29 °C, 0.80 ± 0.11 °C, 1.49 ± 0.64 °C, 1.61 ± 0.64 °C, respectively. The regional cooling in the Amazon, CW-Africa and NA-Boreal is mainly caused by AEROSOL–OCEAN feedbacks. In the E-US the relative role of AEROSOL–LAND *versus* AEROSOL–OCEAN in causing the annual average surface cooling is 35 : 65%.

Aerosols cause substantial drying in CW-Africa (-0.33 ± 0.12 mm per day; -10%), E-US (-0.14 ± 0.22 mm per day; -5%) and NA-Boreal (-0.14 ± 0.09 mm per day; -9%). In the Amazon, aerosols do not have a statistically significant

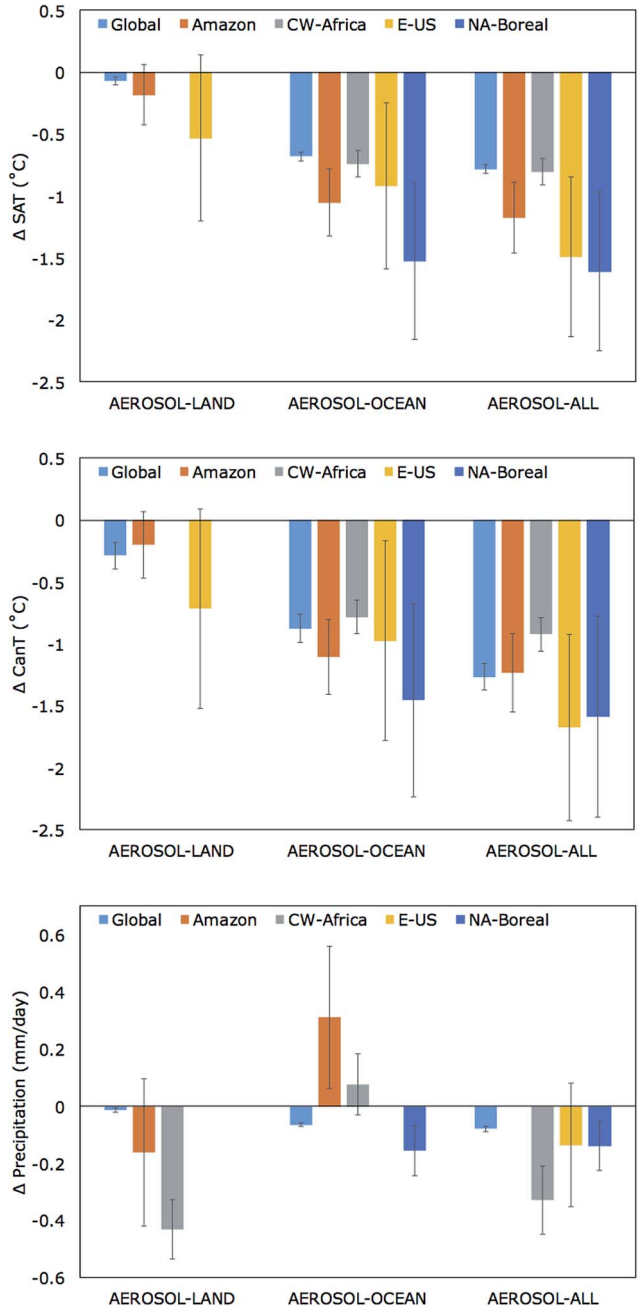

Fig. 4 Summary of annual average aerosol impacts on surface air temperature (SAT, °C), canopy temperature (CanT, °C), and precipitation (mm per day) in 4 key regions and globally for the 3 feedback cases relative to aerosol-free world in 1996–2005. Vertical axes have different scales. Error bars represent ±1 standard deviation due to interannual variability in the climate model calculated as standard error of the mean based on 20 model years.

effect on annual precipitation relative to interannual climate variability. However, separately, AEROSOL–LAND feedbacks decrease precipitation by 0.16 ± 0.26 mm per day (−3%), while AEROSOL–OCEAN feedbacks increase precipitation by 0.31 ± 0.25 (6%). For both the tropical regions, AEROSOL–LAND (drying) and AEROSOL–OCEAN (wetting) feedbacks have opposite sign impacts on precipitation. In CW-Africa, the strong drying is controlled by AEROSOL–LAND feedbacks (Fig. 3). The large reduction in surface visible radiation (Section 3.2) reduces surface evaporation. In addition, atmospheric heating from black carbon aerosols stabilizes the atmospheric column and reduces convection. In NA-Boreal, the drying is driven by AEROSOL–OCEAN feedbacks.

3.4 Aerosol climate change impacts on GPP, R_a and NPP

In CTRL, the global mean annual average GPP = 125.7 ± 1.5 PgC per year; R_a = 61.5 ± 0.5 PgC per year; and NPP = 64.1 ± 1.0 PgC per year. Soil respiration is 62.3 ± 0.8 PgC per year and NEP is −1.83 ± 0.54 PgC per year. The simulated CTRL land carbon fluxes for 1996–2005 are fully consistent with ensemble means from a recent multi-model assessment for the period 1990–2009.[2] At the global scale, relative to the aerosol-free world in 1996–2005, aerosol climate impacts on the land ecosystem services are small due to strongly contrasting sign responses in the tropical and boreal biomes (Fig. 5). Spatially, aerosol impacts on R_a and NPP are similar to the GPP responses (Fig. 5). The global-average impacts result in small reductions in GPP of −2.4 ± 2.0 PgC per year (−2%), in R_a of −2.4 ± 0.7 PgC per year (−4%), and no statistically significant impact on NPP. This finding is in

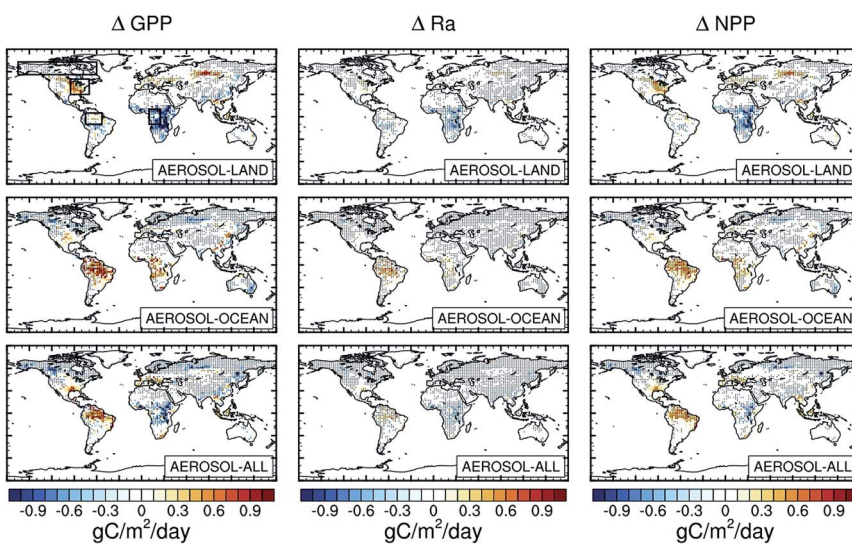

Fig. 5 Spatial distribution of annual average aerosol climate impacts on land ecosystem services (GPP, R_a, and NPP) for the 3 feedback cases relative to aerosol-free world in 1996–2005 (gC per m^2 per day; m^2 refers to area of vegetated land). Dots indicate areas where aerosol impacts are statistically significant at the 95% confidence level. The 4 key regions are defined in the top left panel: Amazon, Central West Africa (CW-Africa), Eastern US (E-US), and North American Boreal (NA-Boreal).

agreement with a previous study using CCSM3.1, which concluded that aerosols do not significantly impact the globally averaged carbon cycle.[31]

Yet, the global-average results conceal substantial opposing regional impacts on land ecosystem services (Fig. 6). In the Amazon, aerosol cooling drives increases in GPP (0.36 ± 0.30 gC per m^2 per day; 4%), net impacts on R_a are tiny ($\sim$1%), resulting in a boost to NPP of 0.30 ± 0.25 gC per m^2 per day (8%). Integrating over the Amazon Basin, this enhancement in plant productivity amounts to about 0.76 ± 0.61 PgC per year, a flux of comparable magnitude to anthropogenic CO_2 emissions from global land use change.[73] The Amazon NPP boost from aerosol global cooling is 5–10 times larger than the NPP enhancement of 0.078 to 0.156 PgC per year from localized aerosol diffuse radiation fertilization.[39] We find that an eco-climate teleconnection from the rise in the NH mid-latitude aerosol pollution band is the protection of Amazon land ecosystem services. Long-term AEROSOL–OCEAN feedbacks control this benefit to Amazon ecosystem health.

A different tropical regime emerges in CW-Africa where AEROSOL–LAND feedbacks control the overall aerosol impacts on land ecosystem services. Potential benefits to plant productivity from regional aerosol cooling associated with AEROSOL–OCEAN feedbacks are offset by strong reductions in surface visible radiation and drying associated with AEROSOL–LAND feedbacks. In this region, aerosols dampen GPP with decreases of 0.23 ± 0.17 gC per m^2 per day (-3%), and R_a with decreases of 0.17 ± 0.06 gC per m^2 per day (-5%), resulting in no statistically significant impact on NPP.

In the E-US temperate zone, aerosol climate effects do not significantly impact GPP and R_a relative to interannual climate variability, but result in NPP enhancements of 0.14 ± 0.22 gC per m^2 per day (6%). At the same time, aerosols decrease the growing season length by 5.1 days relative to the aerosol-free world. Our results suggest that the NPP enhancements are mostly associated with AEROSOL–LAND feedbacks: aerosol diffuse radiation increase of 5% and aerosol cooling outweigh the detrimental effects of slight regional drying, leading to the net NPP enhancement.

The strong aerosol-induced cooling and drying in the NA-Boreal region, driven mainly by AEROSOL–OCEAN feedbacks, leads to the largest fractional changes in land ecosystem services of all the regions. Opposite to the Amazon where the cooling supports GPP and NPP enhancements, the aerosol cooling and drying in NA-Boreal results in GPP decreases of 0.27 ± 0.06 gC per m^2 per day (-35%), R_a decreases of 0.08 ± 0.02 gC per m^2 per day (-32%), and NPP decreases of 0.19 ± 0.05 gC per m^2 per day (-37%), relative to the aerosol-free world. Integrating over the NA-Boreal region, the aerosol-driven dampening of plant productivity amounts to -0.45 ± 0.11 PgC per year.

3.5 Aerosol climate change impacts on isoprene emission

In CTRL, the global mean annual average ISO-P $= 410.8 \pm 4.8$ TgC per year and ISO-M $= 381.9 \pm 2.4$ TgC per year. The simulated global source functions are at the low end of the range of previous estimates.[6] At the global-scale, aerosol cooling of the climate state reduces ISO-P by -30.5 ± 7.0 TgC per year (-7%) and ISO-M by -45.9 ± 4.7 TgC per year (-12%). ISO-P changes follow those of GPP, temperature and surface radiation, while ISO-M is more directly related to

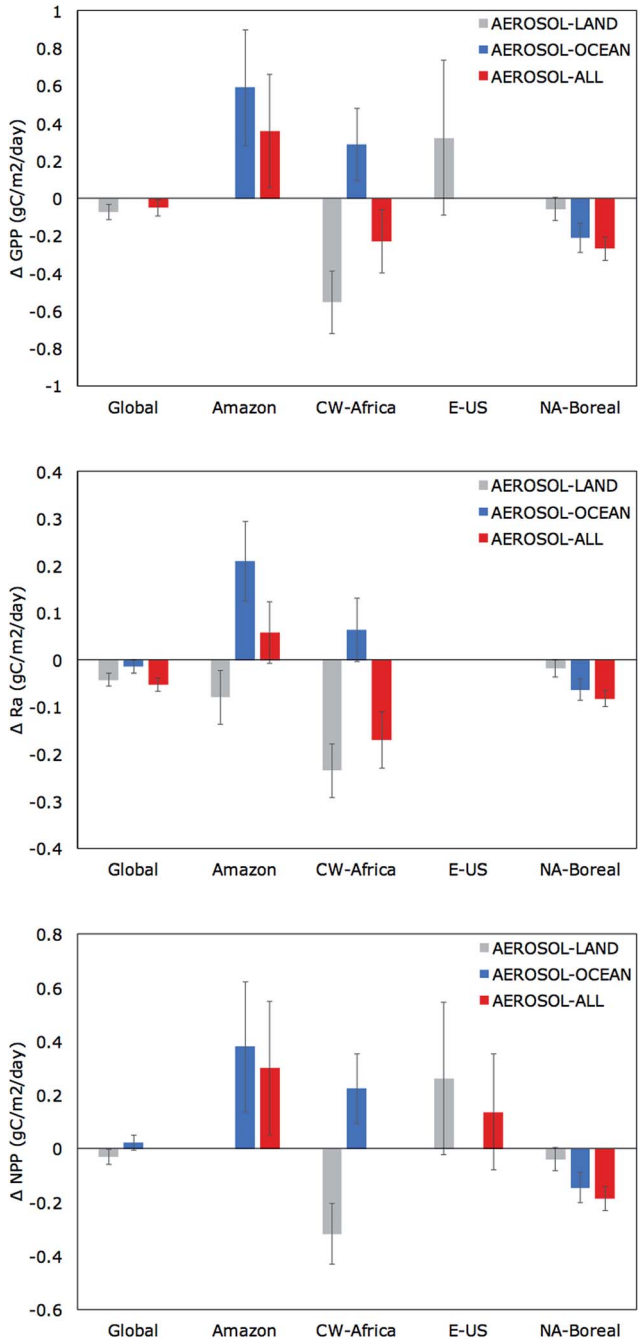

Fig. 6 Summary of annual average aerosol climate impacts on land ecosystem services (GPP, R_a, and NPP) in 4 key regions and globally for the 3 feedback cases relative to aerosol-free world in 1996–2005 (gC per m^2 per day; m^2 refers to area of vegetated land). Vertical axes have different scales. Error bars represent ±1 standard deviation due to interannual variability in the climate model calculated as standard error of the mean based on 20 model years.

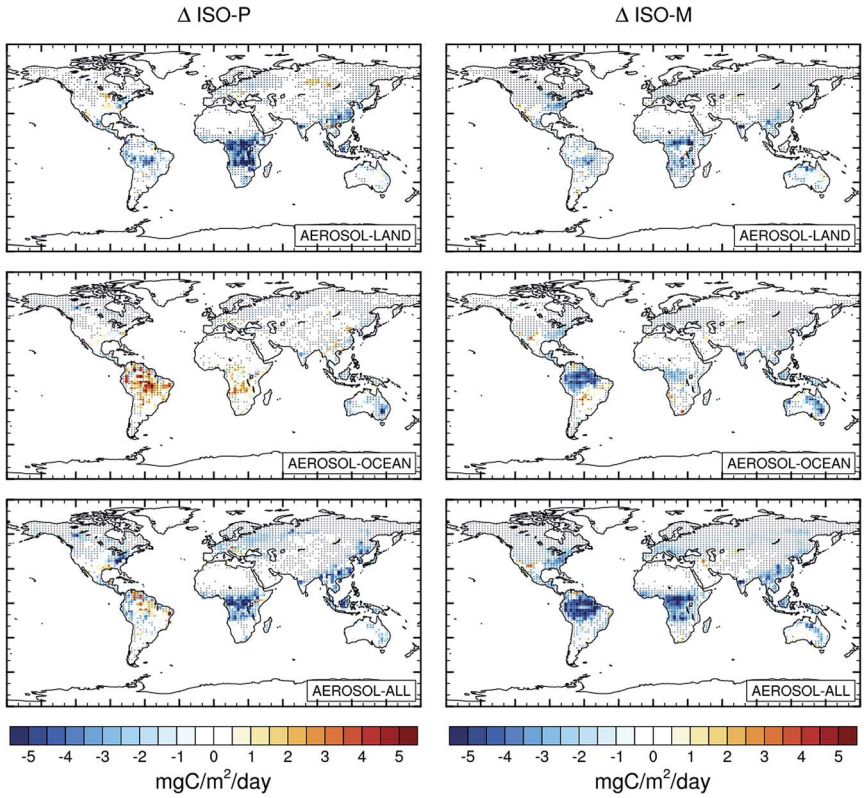

Fig. 7 Spatial distribution of annual average aerosol climate impacts on isoprene emission for 2 emission models (ISO-P and ISO-M) for the 3 feedback cases relative to aerosol-free world in 1996–2005 (mgC per m^2 per day; m^2 refers to area of vegetated land). Dots indicate areas where aerosol impacts are statistically significant at the 95% confidence level.

temperature and surface radiation changes (Fig. 7). Aerosol impacts on plant productivity influence ISO-M indirectly through changes to LAI.

Regional responses are summarized in Fig. 8. In the Amazon, ISO-P is not significantly altered by aerosols relative to interannual climate variability. Aerosol-induced GPP increases, which tend to drive increases in ISO-P, are offset by the effects of regional cooling on isoprene emission. For example, AEROSOL–LAND decreases ISO-P by 1.62 ± 1.28 mgC per m^2 per day (−4%) and AEROSOL–OCEAN increases ISO-P by 1.77 ± 1.41 mgC per m^2 per day (4%). The ISO-M algorithm suggests strong decreases in Amazon isoprene emission of 4.32 ± 1.23 mgC per m^2 per day (−11%) in direct response to aerosol cooling, dominated by AEROSOL–OCEAN feedbacks in this region. In CW-Africa, the strong reduction in surface visible radiation predominantly due to AEROSOL–LAND feedbacks results in overall similar responses of isoprene emission algorithms to the aerosol effects in this region: ISO-P decreases by 2.86 ± 0.59 mgC per m^2 per day (−11%) and ISO-M by 3.56 ± 0.39 mgC per m^2 per day (−13%). In the E-US, ISO-P is decreased by 1.14 ± 0.98 mgC per m^2 per day (−9%), even though NPP increases by 6% in this region. ISO-M is reduced by 1.76 ± 0.84 mgC per m^2 per day (−17%).

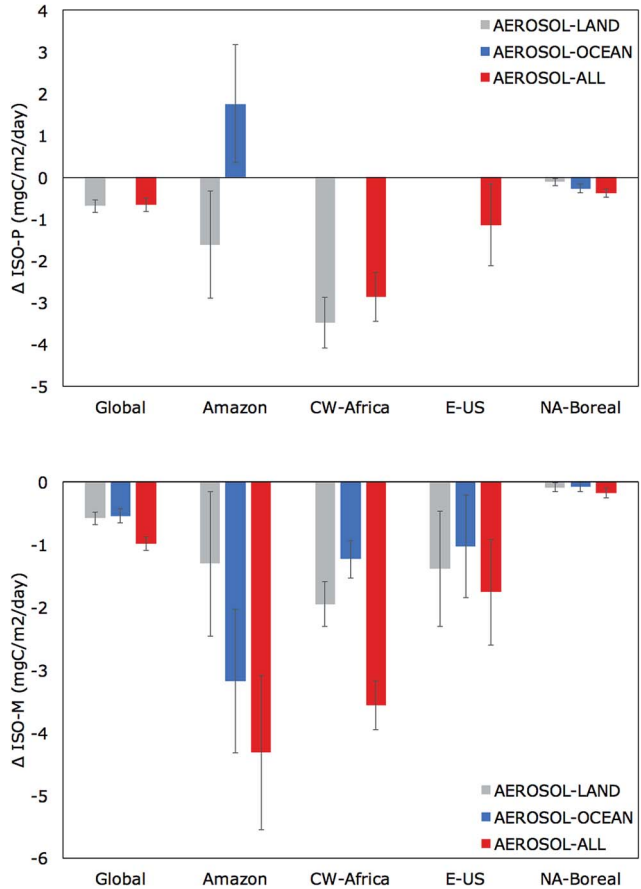

Fig. 8 Summary of annual average aerosol climate impacts on isoprene emission for 2 emission models (ISO-P and ISO-M) in 4 key regions and globally for the 3 feedback cases relative to aerosol-free world in 1996–2005 (mgC per m^2 per day; m^2 refers to area of vegetated land). Vertical axes have different scales. Error bars represent ±1 standard deviation due to interannual variability in the climate model calculated as standard error of the mean based on 20 model years.

Here, aerosol regional dimming and cooling drive the isoprene reductions in both algorithms. At higher latitudes in the NA-Boreal, ISO-P is decreased by 0.38 ± 0.09 mgC per m^2 per day (−56%) while ISO-M is decreased by 0.17 ± 0.08 mgC per m^2 per day (−30%). The larger response in ISO-P reflects the additional role of the decreases in GPP on top of the direct effects of the cooling.

The aerosol-induced reductions in isoprene emission (and monoterpene emission, not shown) are expected to cause a decrease in the BSOA loading representing a negative climate feedback. Despite these aerosol-induced reductions in the BVOC precursor source emissions of BSOA, in fact, anthropogenic pollution causes an overall increase in the BSOA loading (-0.10 W m^{-2}). The dependence of the BSOA production on the pre-existing organic aerosol availability from fossil, biofuel and biomass burning sources completely offsets the impacts of reduced BVOCs and results in an overall increase in BSOA loading in response to

anthropogenic aerosol pollution. Meteorological feedbacks on BSOA production are smaller. Hence, the anthropogenic–biogenic aerosol feedback is positive according to this model; anthropogenic air pollution results in an increased loading of biogenic aerosol.

4. Discussion and conclusions

We applied the NASA ModelE2-YIBs global aerosol–carbon–climate model to quantify the anthropogenic aerosol climate change effects on GPP, R_a and NPP. This study considers all fossil fuel, biofuel and biomass burning aerosol sources as anthropogenic. Our objective was to gain insights into the separate and combined roles of fast feedbacks associated with the land energy exchange and slow feedbacks associated with the ocean energy exchange. We present our annual average aerosol impact results for the 1996–2005 world relative to the hypothetical 1996–2005 world in the absence of the historical rise in aerosol pollution. Globally, we find that aerosols decrease direct and total surface visible radiation by −11% and −3%, respectively, and increase diffuse light by 1–2%. Relative to the aerosol-free world, aerosols cool and dry the global climate system by about −0.8 °C and −0.08 mm per day. At the global-scale, aerosol climate effects on GPP, R_a and NPP are small due to strongly contrasting large effects in tropical and boreal biomes. To first order, aerosol climate effects in different biomes are the reverse of CO_2 climate effects:[7] increases (decreases) in tropical and temperate regions and decreases (increases) in boreal regions. Aerosol slow feedbacks associated with the ocean strongly dominate impacts in the Amazon and North American Boreal. Aerosol fast feedbacks associated with the land play a more important role in the temperate zone and Central Africa where high levels of aerosols and vegetation are co-located. Aerosol-induced changes in temperature and precipitation completely overwhelm the impacts of aerosol diffuse radiation fertilization on land ecosystem services in all regions except the eastern US and areas in the temperate zone.

Aerosol–ocean energy exchange cools the Amazon by −1.2 °C relative to the aerosol-free world. This cooling drives GPP increases of 4% and NPP increases of 8%. The Amazon NPP boost, mostly caused by the long-range climate cooling effect of the NH mid-latitude reflective pollution layer that is transmitted through the ocean, is about 5–10 times larger than estimates of local aerosol diffuse radiation fertilization due to biomass burning in the region. Conversely, in the North American Boreal, aerosol-induced cooling and drying (−1.6 °C, −0.14 mm per day), again mostly through ocean feedbacks, dampen GPP and NPP by about −35% relative to the aerosol-free world in this region. In the eastern US, aerosol increases in diffuse radiation of 5% and cooling of −1.5 °C drive NPP increases of 6% relative to the aerosol-free world. We examined impacts on isoprene emission using 2 conceptually different emission algorithms. Our results suggest global reductions in isoprene emission of 7–12% mostly driven by aerosol cooling. The isoprene impact is algorithm dependent in the Amazon region. For the photosynthesis-dependent isoprene emission model, aerosols have no significant impacts on isoprene in the Amazon due to compensating influences of GPP increases and cooling. Our results suggest aerosol decreases of −11 to −13% in Central West Africa, −9 to −17% in the eastern US, and −30 to −56% in the North American Boreal. Aerosol-induced surface cooling and decreases in isoprene

emission imply reductions in high surface ozone episodes relative to the aerosol-free world.[74] Aerosol pollution climate effects have a hidden benefit of protecting humans and ecosystems from worse ozone health damage.

Our analyses have been performed using a single global Earth system model framework and are subject to uncertainties and limitations. An impact uncertainty measure has been provided relative to interannual climate variability in the model. Our study focuses on aerosol physical climate forcing and does not address aerosol deposition of nutrients to land ecosystems. YIBs does not currently include dynamic C–N coupling, which may potentially lead to enhanced GPP and NPP climate sensitivities. We do not account for feedbacks from altered atmospheric CO_2 concentrations ("carbon-concentration feedbacks") due to the aerosol impacts. However, we speculate that the impacts on global CO_2 concentration are likely to be small, especially based on the minor to negligible global impacts on GPP and NPP. The climate response of soil carbon, and therefore net ecosystem exchange, is still under experimental investigation and associated with large uncertainties.

Aggressive air pollution abatement and climate stabilization strategies that reduce cooling aerosols are essential to protect public health. Yet, our results suggest that tropical and temperate land ecosystem health is currently benefiting from the rise in aerosol pollution. The only logical conclusion is that efforts to reduce the atmospheric aerosol increase the urgency to reduce CO_2 emissions.

Acknowledgements

The authors thank D. Rothenberg for assistance with CMIP5 data. The authors are grateful to C. Wang and W. R. Boos for helpful discussions.

References

1 C. Beer, M. Reichstein, E. Tomelleri, P. Ciais, M. Jung, N. Carvalhais, C. Rodenbeck, M. A. Arain, D. Baldocchi, G. B. Bonan, A. Bondeau, A. Cescatti, G. Lasslop, A. Lindroth, M. Lomas, S. Luyssaert, H. Margolis, K. W. Oleson, O. Roupsard, E. Veenendaal, N. Viovy, C. Williams, F. I. Woodward and D. Papale, *Science*, 2010, **329**, 834–838.

2 S. Sitch, P. Friedlingstein, N. Gruber, S. D. Jones, G. Murray-Tortarolo, A. Ahlström, S. C. Doney, H. Graven, C. Heinze, C. Huntingford, S. Levis, P. E. Levy, M. Lomas, B. Poulter, N. Viovy, S. Zaehle, N. Zeng, A. Arneth, G. Bonan, L. Bopp, J. G. Canadell, F. Chevallier, P. Ciais, R. Ellis, M. Gloor, P. Peylin, S. L. Piao, C. Le Quéré, B. Smith, Z. Zhu and R. Myneni, *Biogeosciences*, 2015, **12**, 653–679.

3 T. D. Sharkey and E. L. Singsaas, *Nature*, 1995, **374**, 769–769.

4 K. Behnke, M. Loivamäki, I. Zimmer, H. Rennenberg, J.-P. Schnitzler and S. Louis, *Photosynth. Res.*, 2010, **104**, 5–17.

5 C. E. Vickers, J. Gershenzon, M. T. Lerdau and F. Loreto, *Nat. Chem. Biol.*, 2009, **5**, 283–291.

6 A. Guenther, T. Karl, P. Harley, C. Wiedinmyer, P. I. Palmer and C. Geron, *Atmos. Chem. Phys.*, 2006, **6**, 3181–3210.

7 P. Ciais, C. Sabine, G. Bala, L. Bopp, V. Brovkin, J. Canadell, A. Chhabra, R. DeFries, J. Galloway, M. Heimann, C. Jones, C. Le Quéré, R. B. Myneni,

S. Piao and P. Thornton, Carbon and Other Biogeochemical Cycles, in *Climate Change 2013: The Physical Science Basis. Contribution of Working Group I to the Fifth Assessment Report of the Intergovernmental Panel on Climate Change*, 2013.

8 P. Friedlingstein, P. Cox, R. Betts, L. Bopp, W. von Bloh, V. Brovkin, P. Cadule, S. Doney, M. Eby, I. Fung, G. Bala, J. John, C. Jones, F. Joos, T. Kato, M. Kawamiya, W. Knorr, K. Lindsay, H. D. Matthews, T. Raddatz, P. Rayner, C. Reick, E. Roeckner, K.-G. Schnitzler, R. Schnur, K. Strassmann, A. J. Weaver, C. Yoshikawa and N. Zeng, *J. Clim.*, 2006, **19**, 3337–3353.

9 C. Yi, D. Ricciuto, R. Li, J. Wolbeck, X. Xu, M. Nilsson, L. Aires, J. D. Albertson, C. Ammann, M. A. Arain, A. C. de Araujo, M. Aubinet, M. Aurela, Z. Barcza, A. Barr, P. Berbigier, J. Beringer, C. Bernhofer, A. T. Black, P. V. Bolstad, F. C. Bosveld, M. S. J. Broadmeadow, N. Buchmann, S. P. Burns, P. Cellier, J. Chen, J. Chen, P. Ciais, R. Clement, B. D. Cook, P. S. Curtis, D. B. Dail, E. Dellwik, N. Delpierre, A. R. Desai, S. Dore, D. Dragoni, B. G. Drake, E. Dufrêne, A. Dunn, J. Elbers, W. Eugster, M. Falk, C. Feigenwinter, L. B. Flanagan, T. Foken, J. Frank, J. Fuhrer, D. Gianelle, A. Goldstein, M. Goulden, A. Granier, T. Grünwald, L. Gu, H. Guo, A. Hammerle, S. Han, N. P. Hanan, L. Haszpra, B. Heinesch, C. Helfter, D. Hendriks, L. B. Hutley, A. Ibrom, C. Jacobs, T. Johansson, M. Jongen, G. Katul, G. Kiely, K. Klumpp, A. Knohl, T. Kolb, W. L. Kutsch, P. Lafleur, T. Laurila, R. Leuning, A. Lindroth, H. Liu, B. Loubet, G. Manca, M. Marek, H. A. Margolis, T. A. Martin, W. J. Massman, R. Matamala, G. Matteucci, H. McCaughey, L. Merbold, T. Meyers, M. Migliavacca, F. Miglietta, L. Misson, M. Mölder, J. Moncrieff, R. K. Monson, L. Montagnani, M. Montes-Helu, E. Moors, C. Moureaux, M. M. Mukelabai, J. W. Munger, M. Myklebust, Z. Nagy, A. Noormets, W. Oechel, R. Oren, S. G. Pallardy, K. T. Pawu, J. S. Pereira, K. Pilegaard, K. Pintér, C. Pio, G. Pita, T. L. Powell, S. Rambal, J. T. Randerson, C. von Randow, C. Rebmann, J. Rinne, F. Rossi, N. Roulet, R. J. Ryel, J. Sagerfors, N. Saigusa, M. J. Sanz, G.-S. Mugnozza, H. P. Schmid, G. Seufert, M. Siqueira, J.-F. Soussana, G. Starr, M. A. Sutton, J. Tenhunen, Z. Tuba, J.-P. Tuovinen, R. Valentini, C. S. Vogel, J. Wang, S. Wang, W. Wang, L. R. Welp, X. Wen, S. Wharton, M. Wilkinson, C. A. Williams, G. Wohlfahrt, S. Yamamoto, G. Yu, R. Zampedri, B. Zhao and X. Zhao, *Environ. Res. Lett.*, 2010, **5**, 34007.

10 P. Friedlingstein, M. Meinshausen, V. K. Arora, C. D. Jones, A. Anav, S. K. Liddicoat and R. Knutti, *J. Clim.*, 2014, **27**, 511–526.

11 M. Jung, M. Reichstein, C. R. Schwalm, C. Huntingford, S. Sitch, A. Ahlström, A. Arneth, G. Camps-Valls, P. Ciais, P. Friedlingstein, F. Gans, K. Ichii, A. K. Jain, E. Kato, D. Papale, B. Poulter, B. Raduly, C. Rödenbeck, G. Tramontana, N. Viovy, Y.-P. Wang, U. Weber, S. Zaehle and N. Zeng, *Nature*, 2017, **541**, 516–520.

12 V. K. Arora, G. J. Boer, P. Friedlingstein, M. Eby, C. D. Jones, J. R. Christian, G. Bonan, L. Bopp, V. Brovkin, P. Cadule, T. Hajima, T. Ilyina, K. Lindsay, J. F. Tjiputra and T. Wu, *J. Clim.*, 2013, **26**, 5289–5314.

13 Y. Zheng, N. Unger, M. P. Barkley and X. Yue, *Atmos. Chem. Phys.*, 2015, **15**, 8559–8576.

14 F. Pacifico, G. A. Folberth, C. D. Jones, S. P. Harrison and W. J. Collins, *J. Geophys. Res.: Atmos.*, 2012, **117**, D22302.

15 N. Unger, *J. Geophys. Res.: Atmos.*, 2013, **118**, 13606–13613.

16 C. Morfopoulos, I. C. Prentice, T. F. Keenan, P. Friedlingstein, B. E. Medlyn, J. Penuelas and M. Possell, *Ann. Bot.*, 2013, **112**, 1223–1238.
17 T. D. Sharkey and F. Loreto, *Oecologia*, 1993, **95**, 328–333.
18 T. D. Sharkey and R. K. Monson, *Plant, Cell Environ.*, 2014, **37**, 1727–1740.
19 J. Lelieveld, J. S. Evans, M. Fnais, D. Giannadaki and A. Pozzer, *Nature*, 2015, **525**, 367–371.
20 O. Boucher, D. Randall, P. Artaxo, C. Bretherton, G. Feingold, P. Forster, V. M. Kerminen, Y. Kondo, H. Liao, U. Lohmann, P. Rasch, S. K. Satheesh, S. Sherwood, B. Stevens and X. Y. Zhang, Clouds and Aerosols, in *Climate Change 2013: The Physical Science Basis. Contribution of Working Group I to the Fifth Assessment Report of the Intergovernmental Panel on Climate Change*, Cambridge, United Kingdom and New York, NY, USA, 2013.
21 G. Myhre, D. T. Shindell, F. Breon, W. Collins, J. Fuglestvedt, J. Huang, D. M. Koch, J. F. Lamarque, D. Lee, B. Mendoza, T. Nakajima, A. Robock, G. Stephens, T. Takemura and H. Zhang, Anthropogenic and Natural Radiative Forcing, in *Climate Change 2013: The Physical Science Basis. Contribution of Working Group I to the Fifth Assessment Report of the Intergovernmental Panel on Climate Change*, Cambridge, United Kingdom and New York, NY, USA, 2013.
22 H. Levy, L. W. Horowitz, M. D. Schwarzkopf, Y. Ming, J.-C. Golaz, V. Naik and V. Ramaswamy, *J. Geophys. Res.: Atmos.*, 2013, **118**, 4521–4532.
23 D. Koch, S. E. Bauer, A. Del Genio, G. Faluvegi, J. R. McConnell, S. Menon, R. L. Miller, D. Rind, R. Ruedy, G. A. Schmidt and D. Shindell, *J. Clim.*, 2011, **24**, 2693–2714.
24 V. Ramanathan and Y. Feng, *Proc. Natl. Acad. Sci. U. S. A.*, 2008, **105**, 14245–14250.
25 M. O. Andreae, C. D. Jones and P. M. Cox, *Nature*, 2005, **435**, 1187–1190.
26 Y. Ming and V. Ramaswamy, *J. Clim.*, 2011, **24**, 5125–5133.
27 P. Wu, N. Christidis and P. Stott, *Nat. Clim. Change*, 2013, **3**, 807–810.
28 C. Wang, *Geophys. Res. Lett.*, 2015, **42**, 10876–10884.
29 C. D. Jones, *Geophys. Res. Lett.*, 2003, **30**, 1479.
30 P. M. Cox, P. P. Harris, C. Huntingford, R. A. Betts, M. Collins, C. D. Jones, T. E. Jupp, J. A. Marengo and C. A. Nobre, *Nature*, 2008, **453**, 212–215.
31 N. Mahowald, K. Lindsay, D. Rothenberg, S. C. Doney, J. K. Moore, P. Thornton, J. T. Randerson and C. D. Jones, *Biogeosciences*, 2011, **8**, 387–414.
32 N. Mahowald, *Science*, 2011, **334**, 794–796.
33 L. Gu, *Science*, 2003, **299**, 2035–2038.
34 D. Niyogi, *Geophys. Res. Lett.*, 2004, **31**, L20506.
35 P. H. F. Oliveira, P. Artaxo, C. Pires, S. De Lucca, A. Procópio, B. Holben, J. Schafer, L. F. Cardoso, S. C. Wofsy and H. R. Rocha, *Tellus, Ser. B*, 2007, **59**, 338–349.
36 G. G. Cirino, R. A. F. Souza, D. K. Adams and P. Artaxo, *Atmos. Chem. Phys.*, 2014, **14**, 6523–6543.
37 L. M. Mercado, N. Bellouin, S. Sitch, O. Boucher, C. Huntingford, M. Wild and P. M. Cox, *Nature*, 2009, **458**, 1014–1017.
38 C. Huntingford, P. M. Cox, L. M. Mercado, S. Sitch, N. Bellouin, O. Boucher and N. Gedney, *Philos. Trans. R. Soc., A*, 2011, **369**, 2026–2037.

39 A. Rap, D. V. Spracklen, L. Mercado, C. L. Reddington, J. M. Haywood, R. J. Ellis, O. L. Phillips, P. Artaxo, D. Bonal, N. Restrepo Coupe and N. Butt, *Geophys. Res. Lett.*, 2015, **42**, 4654–4662.
40 S. Strada and N. Unger, *Atmos. Chem. Phys.*, 2016, **16**, 4213–4234.
41 M. Chen and Q. Zhuang, *Tellus, Ser. B*, 2014, **66**, 21808.
42 X. Yue and N. Unger, *Geosci. Model Dev.*, 2015, **8**, 2399–2417.
43 G. A. Schmidt, M. Kelley, L. Nazarenko, R. Ruedy, G. L. Russell, I. Aleinov, M. Bauer, S. E. Bauer, M. K. Bhat, R. Bleck, V. Canuto, Y.-H. Chen, Y. Cheng, T. L. Clune, A. Del Genio, R. de Fainchtein, G. Faluvegi, J. E. Hansen, R. J. Healy, N. Y. Kiang, D. Koch, A. A. Lacis, A. N. LeGrande, J. Lerner, K. K. Lo, E. E. Matthews, S. Menon, R. L. Miller, V. Oinas, A. O. Oloso, J. P. Perlwitz, M. J. Puma, W. M. Putman, D. Rind, A. Romanou, M. Sato, D. T. Shindell, S. Sun, R. A. Syed, N. Tausnev, K. Tsigaridis, N. Unger, A. Voulgarakis, M.-S. Yao and J. Zhang, *J. Adv. Model. Earth Syst.*, 2014, **6**, 1942–2466.
44 M. Wild, D. Folini, C. Schär, N. Loeb, E. G. Dutton and G. König-Langlo, *Clim. Dyn.*, 2013, **40**, 3107–3134.
45 K. W. Oleson, D. M. Lawrence, G. B. Bonan, M. G. Flanne, E. Kluzek, P. J. Lawrence, S. Levis, S. C. Swenson and P. E. Thornton, *Technical Description of version 4.0 of the Community Land Model (CLM)*, Boulder, USA, 2010.
46 G. D. Farquhar, S. von Caemmerer and J. A. Berry, *Planta*, 1980, **149**, 78–90.
47 J. T. Ball, I. E. Woodrow and J. A. Berry, in *Progress in Photosynthesis Research*, Springer, Netherlands, Dordrecht, 1987, pp. 221–224.
48 S. von Caemmerer and G. D. Farquhar, *Planta*, 1981, **153**, 376–387.
49 A. D. Friend and N. Y. Kiang, *J. Clim.*, 2005, **18**, 2883–2902.
50 N. Unger, K. Harper, Y. Zheng, N. Y. Kiang, I. Aleinov, A. Arneth, G. Schurgers, C. Amelynck, A. Goldstein, A. Guenther, B. Heinesch, C. N. Hewitt, T. Karl, Q. Laffineur, B. Langford, K. A. McKinney, P. Misztal, M. Potosnak, J. Rinne, S. Pressley, N. Schoon and D. Serça, *Atmos. Chem. Phys.*, 2013, **13**, 10243–10269.
51 X. Yue and N. Unger, *Atmos. Chem. Phys.*, 2014, **14**, 9137–9153.
52 X. Yue, N. Unger and Y. Zheng, *Atmos. Chem. Phys.*, 2015, **15**, 11931–11948.
53 R. J. Griffin, D. R. Cocker, J. H. Seinfeld and D. Dabdub, *Geophys. Res. Lett.*, 1999, **26**, 2721–2724.
54 N. Unger, *Geophys. Res. Lett.*, 2014, **41**, 8563–8569.
55 D. Koch, G. A. Schmidt and C. V. Field, *J. Geophys. Res.*, 2006, **111**, D06206.
56 R. L. Miller, G. A. Schmidt, L. S. Nazarenko, N. Tausnev, S. E. Bauer, A. D. DelGenio, M. Kelley, K. K. Lo, R. Ruedy, D. T. Shindell, I. Aleinov, M. Bauer, R. Bleck, V. Canuto, Y. Chen, Y. Cheng, T. L. Clune, G. Faluvegi, J. E. Hansen, R. J. Healy, N. Y. Kiang, D. Koch, A. A. Lacis, A. N. LeGrande, J. Lerner, S. Menon, V. Oinas, C. Pérez García-Pando, J. P. Perlwitz, M. J. Puma, D. Rind, A. Romanou, G. L. Russell, M. Sato, S. Sun, K. Tsigaridis, N. Unger, A. Voulgarakis, M.-S. Yao and J. Zhang, *J. Adv. Model. Earth Syst.*, 2014, **6**, 441–478.
57 H. Bian and M. J. Prather, *J. Atmos. Chem.*, 2002, **41**, 281–296.
58 H. Bian, *J. Geophys. Res.*, 2003, **108**, 4242.
59 D. Koch and A. D. Del Genio, *Atmos. Chem. Phys.*, 2010, **10**, 7685–7696.
60 G. Myhre, B. H. Samset, M. Schulz, Y. Balkanski, S. Bauer, T. K. Berntsen, H. Bian, N. Bellouin, M. Chin, T. Diehl, R. C. Easter, J. Feichter, S. J. Ghan,

D. Hauglustaine, T. Iversen, S. Kinne, A. Kirkevåg, J.-F. Lamarque, G. Lin, X. Liu, M. T. Lund, G. Luo, X. Ma, T. van Noije, J. E. Penner, P. J. Rasch, A. Ruiz, Ø. Seland, R. B. Skeie, P. Stier, T. Takemura, K. Tsigaridis, P. Wang, Z. Wang, L. Xu, H. Yu, F. Yu, J.-H. Yoon, K. Zhang, H. Zhang and C. Zhou, *Atmos. Chem. Phys.*, 2013, **13**, 1853–1877.

61 D. T. Shindell, J. F. Lamarque, M. Schulz, M. Flanner, C. Jiao, M. Chin, P. J. Young, Y. H. Lee, L. Rotstayn, N. Mahowald, G. Milly, G. Faluvegi, Y. Balkanski, W. J. Collins, A. J. Conley, S. Dalsoren, R. Easter, S. Ghan, L. Horowitz, X. Liu, G. Myhre, T. Nagashima, V. Naik, S. T. Rumbold, R. Skeie, K. Sudo, S. Szopa, T. Takemura, A. Voulgarakis, J. H. Yoon and F. Lo, *Atmos. Chem. Phys.*, 2013, **13**, 2939–2974.

62 D. T. Shindell, O. Pechony, A. Voulgarakis, G. Faluvegi, L. Nazarenko, J.-F. Lamarque, K. Bowman, G. Milly, B. Kovari, R. Ruedy and G. A. Schmidt, *Atmos. Chem. Phys.*, 2013, **13**, 2653–2689.

63 N. A. Rayner, P. Brohan, D. E. Parker, C. K. Folland, J. J. Kennedy, M. Vanicek, T. J. Ansell and S. F. B. Tett, *J. Clim.*, 2006, **19**, 446–469.

64 J.-F. Lamarque, T. C. Bond, V. Eyring, C. Granier, A. Heil, Z. Klimont, D. Lee, C. Liousse, A. Mieville, B. Owen, M. G. Schultz, D. Shindell, S. J. Smith, E. Stehfest, J. Van Aardenne, O. R. Cooper, M. Kainuma, N. Mahowald, J. R. McConnell, V. Naik, K. Riahi and D. P. van Vuuren, *Atmos. Chem. Phys.*, 2010, **10**, 7017–7039.

65 P. M. Forster, T. Andrews, P. Good, J. M. Gregory, L. S. Jackson and M. Zelinka, *J. Geophys. Res.: Atmos.*, 2013, **118**, 1139–1150.

66 D. T. Shindell, *Nat. Clim. Change*, 2014, **4**, 274–277.

67 A. G. Carlton, R. W. Pinder, P. V. Bhave and G. A. Pouliot, *Environ. Sci. Technol.*, 2010, **44**, 3376–3380.

68 M. Wild, *Bull. Am. Meteorol. Soc.*, 2012, **93**, 27–37.

69 J. Hansen, R. Ruedy, M. Sato and K. Lo, *Rev. Geophys.*, 2010, **48**, RG4004.

70 W. R. Boos and R. L. Korty, *Nat. Geosci.*, 2016, **9**, 892–897.

71 A. J. Broccoli, K. A. Dahl and R. J. Stouffer, *Geophys. Res. Lett.*, 2006, **33**, L01702.

72 J. C. H. Chiang and A. R. Friedman, *Annu. Rev. Earth Planet. Sci.*, 2012, **40**, 383–412.

73 C. Le Quéré, R. Moriarty, R. M. Andrew, J. G. Canadell, S. Sitch, J. I. Korsbakken, P. Friedlingstein, G. P. Peters, R. J. Andres, T. A. Boden, R. A. Houghton, J. I. House, R. F. Keeling, P. Tans, A. Arneth, D. C. E. Bakker, L. Barbero, L. Bopp, J. Chang, F. Chevallier, L. P. Chini, P. Ciais, M. Fader, R. A. Feely, T. Gkritzalis, I. Harris, J. Hauck, T. Ilyina, A. K. Jain, E. Kato, V. Kitidis, K. Klein Goldewijk, C. Koven, P. Landschützer, S. K. Lauvset, N. Lefèvre, A. Lenton, I. D. Lima, N. Metzl, F. Millero, D. R. Munro, A. Murata, J. E. M. S. Nabel, S. Nakaoka, Y. Nojiri, K. O'Brien, A. Olsen, T. Ono, F. F. Pérez, B. Pfeil, D. Pierrot, B. Poulter, G. Rehder, C. Rödenbeck, S. Saito, U. Schuster, J. Schwinger, R. Séférian, T. Steinhoff, B. D. Stocker, A. J. Sutton, T. Takahashi, B. Tilbrook, I. T. van der Laan-Luijkx, G. R. van der Werf, S. van Heuven, D. Vandemark, N. Viovy, A. Wiltshire, S. Zaehle and N. Zeng, *Earth Syst. Sci. Data*, 2015, **7**, 349–396.

74 D. J. Jacob and D. A. Winner, *Atmos. Environ.*, 2009, **43**, 51–63.

